Received: 22 September 2023 | Accepted: 20 May 2024

DOI: 10.1111/mms.13153

ARTICLE

Marine Mammal Science

In vivo viscoelastic properties of cetacean integument: an experimental characterization

Dory Y. Yang[1] | K. Alex Shorter[1] | Michael Moore[2] | Julie Rocho-Levine[3] | Randall S. Wells[4] | Kira Barton[1] | Mark Johnson[5]

[1]Department of Mechanical Engineering, University of Michigan, Ann Arbor, Michigan

[2]Biology Department, Woods Hole Oceanographic Institution, Woods Hole, Massachusetts

[3]Dolphin Quest Oahu, Honolulu, Hawaii

[4]Chicago Zoological Society's Sarasota Dolphin Research Program, c/o Mote Marine Laboratory, Sarasota, Florida

[5]Zoophysiology, University of Aarhus, Aarhus, Denmark

Correspondence
K. Alex Shorter, 3534 GGB, 2350 Hayward, Ann Arbor, MI 48109.
Email: kshorter@umich.edu

Funding information
National Oceanographic Partnership Program, Grant/Award Number: N00014-11-1-0113

Abstract

Suction cups are commonly used to attach biologging tags to cetaceans, and interact mechanically with compliant integument, an organ primarily composed of skin and blubber. However, the impact of compliance on suction cup performance is difficult to predict because knowledge about in vivo integument mechanics is lacking. Here, an experimental approach is used to investigate the mechanical properties of common bottlenose dolphin (*Tursiops truncatus*) integument using a custom instrument, the static suction cup (SSCup), to collect data from both trained dolphins and wild individuals ($n = 17$) during a static pose. Three loading profiles were applied at three sites to quantify nonlinear stiffness, hysteresis, and creep. The site at the dorsal fin insertion exhibited the highest stiffness, while sites posterior to the blowhole and above the pectoral fin showed greater energy dissipation during cyclic loading. Viscoelastic behavior was observed across all sites. Suction cup performance on a surrogate material with broadly similar compliance showed reduced performance compared to cups on rigid acrylic: the maximum applied force at detachment on acrylic (50 N) was twice as large as the compliant substrate (25 N). Site-dependent compliance of integument may lead

This is an open access article under the terms of the Creative Commons Attribution-NonCommercial License, which permits use, distribution and reproduction in any medium, provided the original work is properly cited and is not used for commercial purposes.
© 2024 The Author(s). *Marine Mammal Science* published by Wiley Periodicals LLC on behalf of Society for Marine Mammalogy.

to varying performance of suction cups as an attachment method for tags.

KEYWORDS
biologging, dolphin integument, dolphin skin, in vivo, suction cup, viscoelasticity

1 | INTRODUCTION

For animals, like cetaceans, that spend most of their lives underwater, body-attached instruments (biologging tags) are essential for monitoring the behavior, movement, and surrounding environment during daily-life. These devices can be broadly divided into two categories: (1) low-power tags that make measurements (GPS, temperature, salinity, depth) over periods that range from weeks to months at relatively low sampling rates and (2) higher-power tags that make high resolution measurements (kinematics, acoustics, video) over the hour to day range. Attachment methods used to secure these tags vary accordingly (Horning et al., 2019). Devices deployed for weeks to months are typically attached using skin-penetrating barbs or bolts, typically transmit sparse dive and movement data via telemetry, and tend not to be recovered. For devices that combine a wider range of sensors (e.g., sound or video) sampled at higher resolution, telemetry is seldom an option and data must be stored in on-board memory necessitating physical recovery of the tag to obtain the data. The increased memory and battery consumption of high-resolution multisensor tags generally constrain operating duration to a few days. For such short durations skin-penetrating attachment is ethically difficult and suction cups have been the preferred method to attach short-term tags, taking advantage of the smoothness of cetacean skin (Hanson & Baird, 1998; Hooker & Baird, 2001). Suction cup tags can be applied by hand to restrained animals, and to free-swimming animals using hand-held poles, UAVs, or a ballistic delivery, and can be released at a programmable time using corrosive wire links, leaving no equipment on the animal (Johnson & Tyack, 2003; Kleivane et al., 2022; Wiley et al., 2023). However, the vacuum force in the cups inevitably weakens as fluid leaks into the sealed volume over time, making the cups increasingly vulnerable to dislodgement due to external forces from high-speed swimming, twisting, and turning, acrobatics, contact with other animals or with the sea floor.

Leakage rates are variable and may be exacerbated by poor skin condition, e.g., due to sloughing, scarring or biofilm growth. The resulting unpredictable longevity of tags complicates experiment design and is particularly problematic for controlled exposure experiments that require set durations of preexposure, exposure, and postexposure conditions (Isojunno et al., 2018). Several types and sizes of suction cups have been used on cetaceans, from large stiff rubber cups designed to attach roof-racks to cars (Schneider et al., 1998), through to small soft silicone cups (Johnson & Tyack, 2003), raising the question of whether the material and shape of cups influence their attachment tenacity. An analysis of in vivo cup performance on cetaceans is not available, but cup mechanics have been explored for applications in the packaging industry (Mantriota & Messina, 2011) and for robots designed for climbing on engineered surfaces (Aslam & Dangi, 2005; Bahr et al., 1996; Liu et al., 2006; Miyake et al., 2007, 2009; Rutkowski et al., 2009). These experimental studies have been complemented by models used to estimate adhesion and friction force of a deformed cup (Ge et al., 2015; Liu et al., 2006). However, these studies focus on systems that actively create attachment forces using pumps. For cetaceans, the weight, power consumption and complexity of a vacuum pump are difficult to accommodate leading almost exclusively to the use of passive suction cups in biologging tags.

Passive suction cups attach to a surface by creating a pressure differential (ΔP) between the ambient environment (with pressure p_o) and the interior volume of the cup (with pressure p_v), Figure 1. During attachment, an

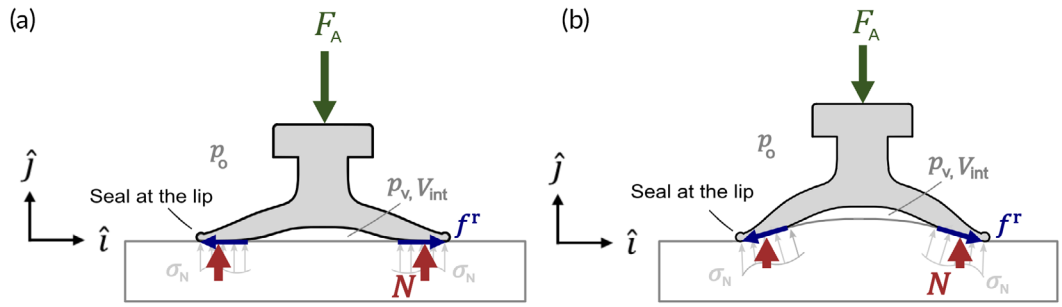


FIGURE 1 An illustration of suction cup mechanics on a (a) rigid and (b) compliant substrate. The material properties of the cup and substrate both contribute to the initial configuration and forces generated by the cup. In the diagrams, p_o is the environmental pressure acting on the cup, p_v and V_{int} are the internal pressure and the internal volume of the cup, respectively. f^r is the resistive force tangential to the contact surface between the cup and substrate. Changes to the internal volume (V_{int}) influence the internal pressure (p_v) and the pressure differential (ΔP), which in turn determines the magnitude of the attachment force (F_A) and the normal stress (σ_N), i.e., normal force (N) between the lip of the cup and the attachment surface.

external force deforms the cup, flattening the lip onto the surface and expelling most of the air within the interior volume. The shape deformation of the elastomeric material of the cup stores energy during attachment, and after the external force is relaxed, work to restore the cup to its undeformed configuration. As the cup attempts to return to its original shape, the lip acts as a check valve preventing ingress of the surrounding fluid. The seal at the lip, and the increasing internal volume (V_{int}) resulting from cup relaxation, create a pressure differential (ΔP) and corresponding attachment force (F_A). The internal volume (V_{int}) of the cup continues to expand until a balance is reached between the attachment force (F_A) and the other forces acting on the cup, Figure 1(a). This analysis assumes that the substrate under the cup is perfectly rigid, which is a realistic assumption for the surfaces typically used in engineering applications of cups. But the outer surface (integument) of cetaceans is compliant, leading to a more complex mechanical interaction between the cup and the skin (Figure 1b). In this case, the attachment force (F_A) in the cup pulls the skin surface into the cup, deforming the substrate and reducing the internal volume (V_{int}) of the cup. This reduces the force generated by the cup potentially making the attachment weaker and more liable to be dislodged. Strong deformation of the skin surface can also cause edema that may discomfort the animal and change the local material properties. Thus, the mechanical properties of the integument may have an important impact on the attachment duration of a suction-cup tag.

With cetaceans, cups are attached to the animal's integument, an organ comprising primarily skin, blubber, blood vessels, nerves, and connective tissue (Fish & Rohr, 1999; Fitzgerald & Fitzgerald, 1995; Pavlov, 2006). This system provides protection, thermoregulation, buoyancy, and drag reduction for the animal (Kovacs et al., 2018). Cetacean integument is arranged in epidermal, dermal, and subdermal layers that possess both viscous and elastic (viscoelastic) properties (Pabst, 1996a,b), and may exhibit a nonlinear stress–strain relationship during loading (Ratner et al., 2004). The elements of the integument are nonuniformly distributed and highly integrated, Figure 2(a). While imaging (e.g., CT scan in Figure 2a) has been used to characterize this organ system, there is scant information on the mechanical properties of this material directly relevant to suction cup design, in particular the in vivo deformation of the organ system under vacuum loading. Studies of cetacean integument mechanics have instead relied on material properties measured from ex vivo samples of the composite tissues collected from cadavers (Fitzgerald & Fitzgerald, 1995). Removing the sample from the body inevitably compromises the structural integrity of the composite tissue and ex vivo measurements likely provide a biased representation of the behavior of living integument.

To date, in vivo methods to characterize cetacean integument have been lacking. For human integument, researchers have used a variety of meters (indenter, Pailler-Mattei et al., 2008; and twistometer, Escoffier

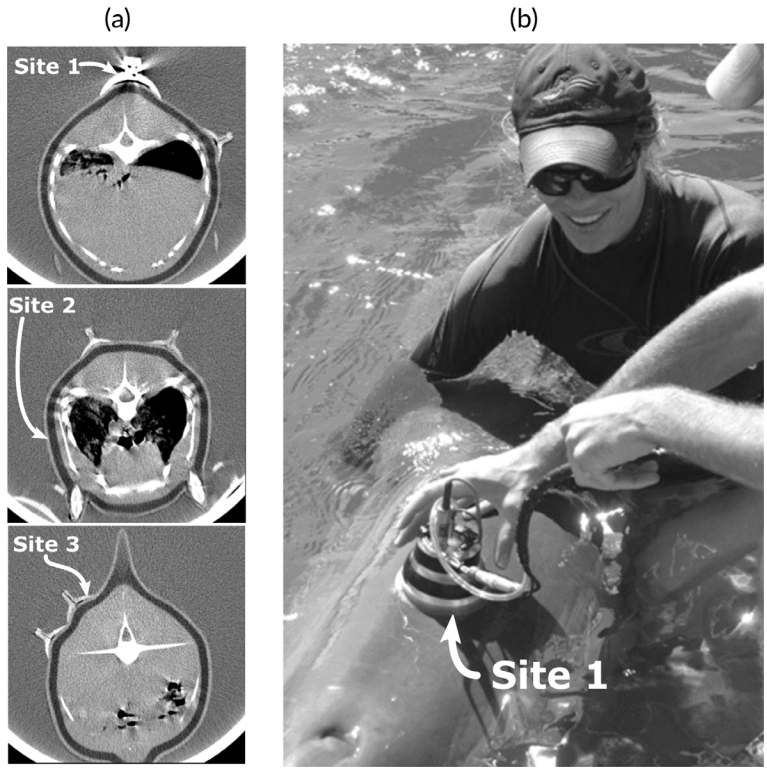


FIGURE 2 (a) Cross sectional CT images from a common dolphin (*Delphinus delphis*) cadaver at the three sites measured with the SSCup. (Site 1) Posterior to the blowhole, a location with significant subcutaneous fat; (Site 2) above the pectoral flipper, which overlies muscle on the blade of the scapula; and (Site 3) near the dorsal fin insertion, which has increased blubber fiber content as part of the dorsal fin saddle. (b) The SScup is shown secured to Site 1 on a representative animal stationing for data collection.

et al., 1989; Sanders, 1973), ultrasound (Bercoff et al., 2004; Diridollou et al., 2000; Nightingale et al., 2002; Sandrin et al., 2003), and multiple optical instruments (light intensity; Cua et al., 1990; Elsner et al., 1990; Weickenmeier et al., 2015), optical coherence topography (OCT; Hendriks et al., 2006), and digital image correlation (DIC; Evans & Holt et al., 2009; Solav et al., 2018) to capture mechanical responses under various loading conditions. Loading has included indentation (Evans & Holt, 2009; Pailler-Mattei et al., 2008; Solav et al., 2018), torsion (Escoffier et al., 1989; Sanders, 1973), acoustic inputs (Bercoff et al., 2004; Nightingale et al., 2002; Sandrin et al., 2003), and suction (Cua et al., 1990; Diridollou et al., 2000; Elsner et al., 1990; Hendriks et al., 2006; Weickenmeier et al., 2015;). Using data from these in vivo experiments, different models have been established (Pailler-Mattei et al., 2008; Takema et al., 1994) to estimate bulk material properties for human integument, such as extensibility and Young's modulus (Escoffier et al., 1989; Sanders, 1973).

Here we build on results in the literature by first characterizing the in vivo compliance of cetacean integument, and then investigating passive suction cup performance on comparable compliant substrates. We seek to answer the following questions: (1) How do the bulk mechanical properties of cetacean integument vary at potential tagging locations on the body? and (2) How is the performance of a suction cup affected by a compliant substrate? To enable our investigation, we developed a system to measure in vivo dolphin integument mechanics and then used the resulting characterizations to interpret suction cup performance on engineered substrates with, and without, compliance. The results indicate ways in which a suction cup can be engineered to improve performance on cetacean integument, potentially leading to increased attachment durations with a lower impact on the animal.

2 | METHODS

We quantified the in vivo response of bottlenose dolphin (*Tursiops truncatus*) integument under vacuum loading using a custom-designed measurement device, the static suction cup (SSCup). This portable system was used to make measurements on animals in human care that were trained to station for data collection (Figure 2b) and on wild dolphins briefly restrained for health assessments. The SSCup was used to mimic suction cup forces by loading integument with a partial vacuum. Viscoelastic properties were quantified using deformation measurements. Suction cup performance as a function of substrate compliance was also investigated using a uniaxial extension machine to load cups to failure when secured to surrogate surfaces. The study protocol for the work with animals was approved by the Woods Hole Oceanographic Institutional Animal Care and Use Committee. Research with wild dolphins in Sarasota Bay was performed under National Marine Fisheries Service Scientific Research Permit No. 20455.

2.1 | Integument characterization

The static suction cup, SSCup, comprises a rigid acrylic half-dome body with a molded silicone lip that creates a sealed volume for vacuum loading. A linear variable differential transformer (LVDT, LT0617; Active Sensors, Indianapolis, IN) measures peak integument displacement during loading. A peristaltic pump (200 series; Williamson Manufacturing, Brighton, UK) creates the controllable vacuum loading inside the chamber via flexible tubing to the SSCup. A pressure transducer (US300; Measurement Specialties, Hampton, VA) measures the differential pressure (ΔP) inside versus outside the chamber, and two thermistors (192-102DEW-A01; Honeywell, Charlotte, NC), one located near the tip of the displacement sensor and the other in the lip of the cup, measure integument temperature during loading. All data were sampled at 10 Hz and were logged using a notebook computer and a USB analog to digital converter (U6; LabJack, Lakewood, CO). The system is battery-powered and enclosed in a splash-proof case for portability.

Experiments were conducted with common bottlenose dolphins (*Tursiops truncatus*; $n = 5$) at Dolphin Quest Oahu (Honolulu, HI) and during catch-and-release dolphin health assessments ($n = 12$) conducted by the Chicago Zoological Society's Sarasota Dolphin Research Program (Sarasota, FL; Wells, 2009; Wells et al., 2004). The mean body mass, length (from the tip of rostrum to the notch of fluke), and girth (at the dorsal fin insertion, where the trunk is the widest) of the animals were 198.8 kg ($SD = 54.2$), 2.54 m ($SD = 0.17$), and 1.39 m ($SD = 0.14$), respectively (Table S1). At Dolphin Quest, animals were trained to station in the water, and maintain a static posture during data collection (Figure 2b). Dolphins in the Sarasota Bay health assessments were resting on a shaded and padded boat deck for veterinary examinations. Displacement measurements were made at three sites on the animals: Site 1: posterior to the blowhole; Site 2: above the pectoral fin; and Site 3: at the dorsal fin insertion, Figure 3(a). Biologging tags are often placed at or near these three sites and have distinct anatomical substructures with varying amounts of subdermal fat, bone, and muscle, Figure 2(a).

Three loading profiles were applied at each site: static step, cyclic, and creep-recovery loading, Figure 3(b). During the static step loading, pressure differential (ΔP) was increased to 30 kPa and then decreased to 0 kPa incrementally: 0, 5, 10, 20, 30, 20, 10, 5, 0 kPa. The pressure differential (ΔP) at each step was held for 45 s to allow the deformation response to reach steady state. This duration was long enough for the measured deformation to reach more than 95% of the measured deformation of longer trials conducted during a preliminary round of analysis. Three levels of cyclic loading were used to dynamically load the integument: low (5–10 kPa), medium (5–20 kPa), and high (5–30 kPa). Twenty-five cycles of each loading level were conducted at each site, starting with the low-level and finishing with the high-level loading. The constant loading rate of the pump (1.2 kPa/s) determined the period of the cyclic loading: low (10 ± 1 s), medium (32 ± 3 s), and high (55 ± 3 s). A creep-recovery loading profile was also used to characterize the time-dependent response of the integument, where pressure was first increased from 0 to 30 kPa at a constant loading rate (1.2 kPa/s), then held at 30 kPa for 95 s before the pressure was released. Results from

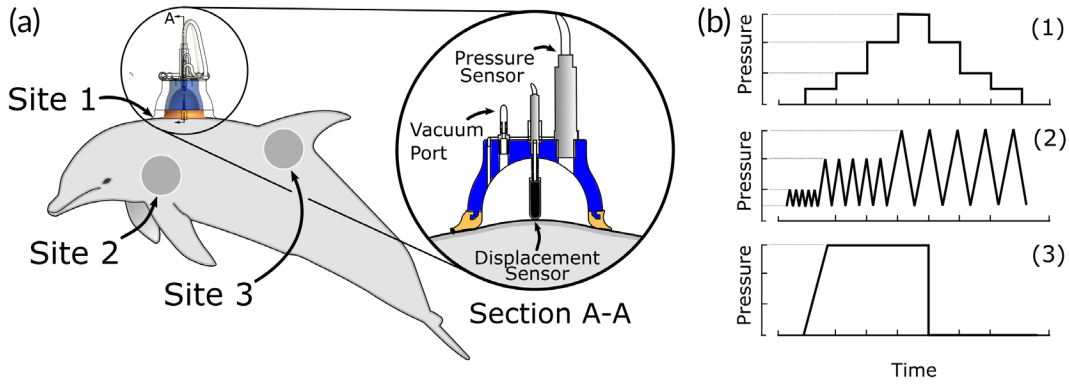


FIGURE 3 (a) Static Suction cup (SSCup) was used to create vacuum loading on the integument during the experiment. Integument deformation was measured with a linear variable differential transformer (LVDT). Three sites on the animals with varying substructure were examined during each trial. (b) Three loading profiles were used with the SSCup during each assessment: (1) A static step loading and unloading profile where each load was held for 45 s; (2) a cyclic loading profile over three pressure ranges; and (3) a creep-recovery loading where the load was applied and then held for 95 s before release.

the three loading profiles at the three sites were then used to quantify the viscoelastic behavior of the integument (Özkaya et al., 2016).

2.2 | Suction cup testing

Suction cup mechanics during normal loading were measured using a uniaxial extension testing machine (4301; Instron, Norwood, MA). Cups were attached to both a rigid acrylic sheet and a compliant integument phantom and loaded until failure (i.e., cups were no longer attached to the substrate). In both cases, the surface was cleaned and wetted with water before cup attachment. The cylindrical integument phantom had a diameter of 95.3 mm and thickness of 44.5 mm and was made from platinum-cured silicone rubber with shore hardness as 00–10 (Ecoflex 00–10; Smooth-On, Inc., Macungie, PA), Figure 4(a). The constant displacement rate of 60 mm/min was used to load the cups, with the resulting applied normal force (F_P) recorded for each trial. A fixed camera (HERO 5; GoPro, San Mateo, CA) recorded cup deformation during the experiment at 25 fps, and a pressure transducer (PX3 Series; Honeywell, Charlotte, NC) measured the differential (ΔP) between ambient environment and the internal cup pressure. Data were logged using a USB microcontroller (Arduino Uno Rev3; Arduino, Italy) and a notebook computer. Ten silicone rubber cups (45 mm diameter, 10.4 mm internal height, custom design manufactured by Da/Pro Rubber, Inc., Broken Arrow, OK) were tested 10 times each on both substrates.

2.3 | Data analysis

2.3.1 | Integument characterization

The magnitude of the loading force (F) created by the SSCup during the trials was calculated using the measured pressure differential (ΔP) and the area at the interface between the instrument and the animal ($A_S = 45.6\ cm^2$) for the static step, cyclic, and creep-recovery loading trials.

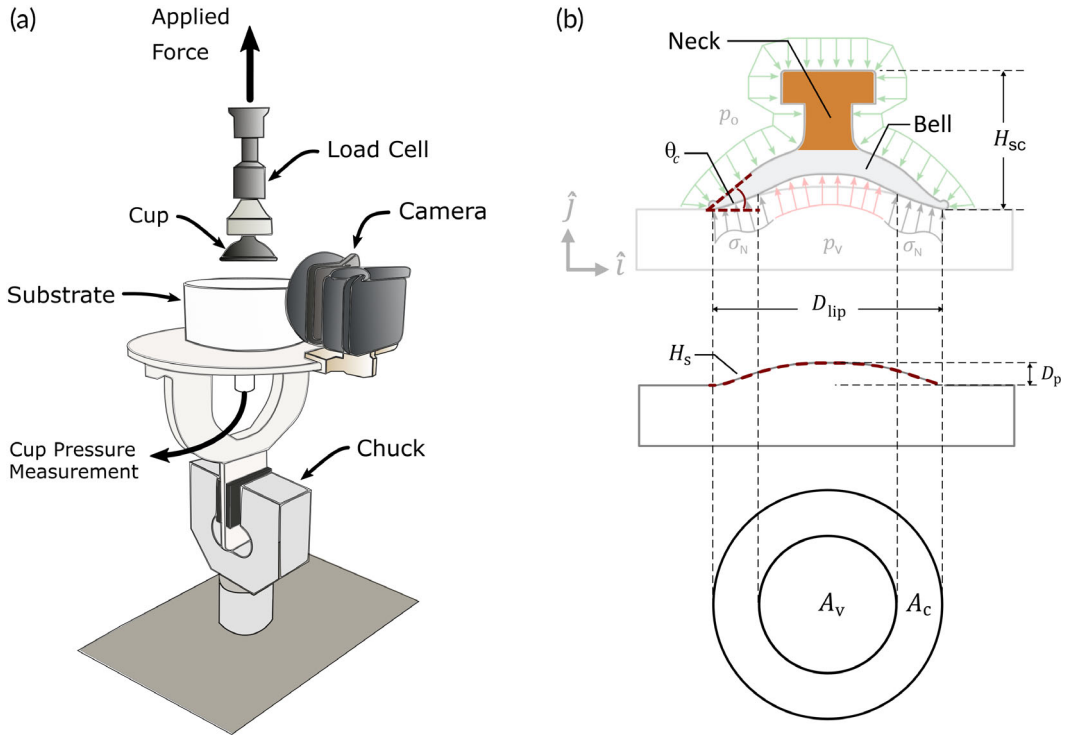


FIGURE 4 (a) A schematic of the experimental setup used to evaluate suction cup performance under normal loading. A universal tester (4301; Instron, Norwood, MA) was used to load the cup at a constant displacement rate (60 mm/min) until failure. Applied force (F_p), system displacement (suction cup and substate), and the pressure differential (ΔP) between the cup and the ambient were measured during the experiment. (b) A suction cup is composed of a neck and a bell, with its projected area divided into vacuum (A_v) and contact (A_c) areas. D_{lip} is the outer diameter of the cup. Contact angle (θ_c) was defined as the angle between the bottom edge of the lip and the tangential line of the bell, and the height of the suction cup (H_{sc}) was measured from the lip to the top of the cup. Peak displacement of the substrate (D_p) was defined as the maximum distance between the loaded substrate profile (H_s) and the initial setup height.

$$F = \Delta P \cdot A_S \tag{1}$$

Steady state displacement (D_{ss}) and the corresponding pressure differential (ΔP) were taken as the average of the measurements during the final 25% of each time step during the static step loading trials. For each trial, force versus displacement (F vs. D_{ss}) data set of each time step during loading and unloading were calculated. 1st-order linear regression was then executed to estimate the stiffness of the integument (k_L and k_U N/m) during loading and unloading, respectively (Figure 5a,b):

$$\hat{F}_L = k_L \hat{D}_{ss} + c_1 \text{ where } \hat{D}_{ss} \in [D_o, D_p] \tag{2}$$

$$\hat{F}_u = k_U \hat{D}_{ss} + c_u \text{where } \hat{D}_{ss} \in [D_p, D_f] \tag{3}$$

$\hat{F}_L - \hat{D}_{ss}$ and $\hat{F}_u - \hat{D}_{ss}$ are the modeled force versus displacement correlation from the 1st-order linear regression. Where D_o, D_p, D_f correspond to the initial, peak, and final steady state displacement (D_{ss}) calculated per the measurements during each trial. k_L, k_U, and c_l, c_u are the coefficients of the 1st-order term and the intercepts for the modeled deformation during loading and unloading, respectively. Figure 5(a,b) showcases the loading and

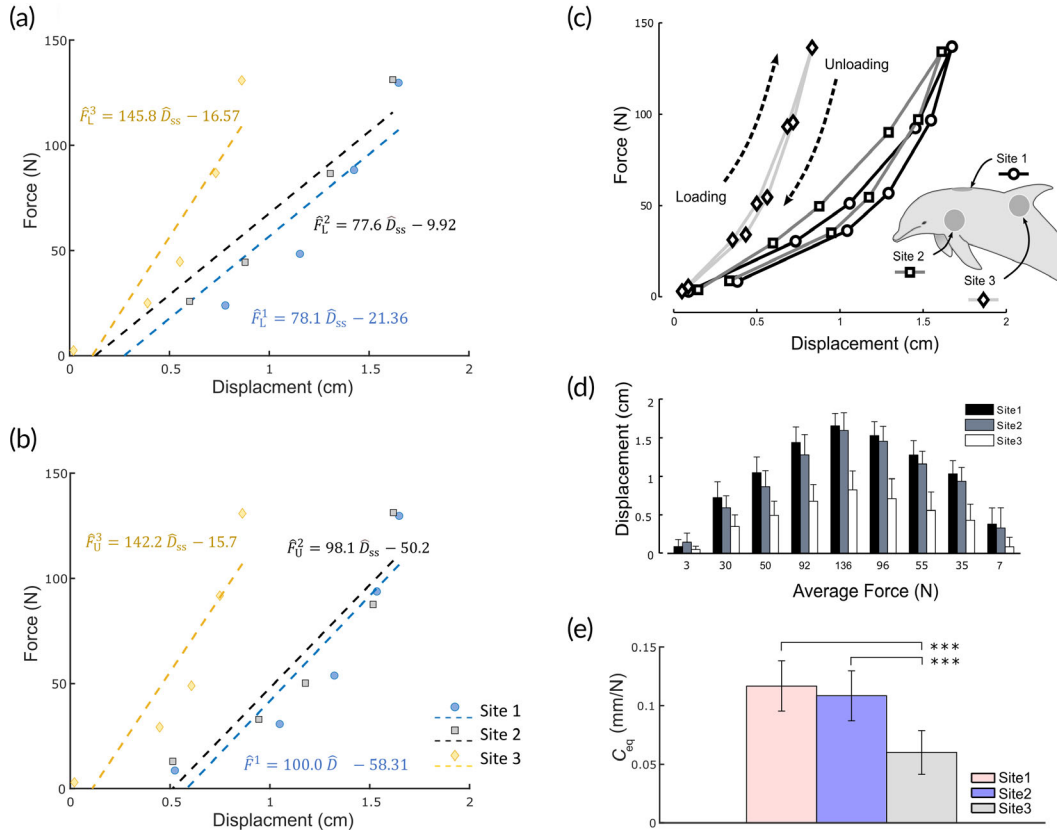


FIGURE 5 Data from each animal were used to fit a 1st-order linear regression model during the steady state loading and unloading. Data and fit for a representative animal (TT01) are presented for (a) loading and (b) unloading sections. The fit was used to calculate the corresponding average stiffness ($\overline{S}_i$; Equation 4) and the equivalent compliance ($C_{eq,i}$; Equation 5). (c) Average steady state force versus displacement curves for the three loading sites. Sites 1 and 2 showed more compliance and hysteresis than Site 3. (d) Average steady state displacement under the nine loading steps, along with standard deviation. The deformations at Sites 1 and 2 were larger than those measured at Site 3 under all loading conditions. (e) *t*-test results indicate the equivalent compliance (C_{eq}) at Site 3 exists at a very highly significant (***) difference compared to Site 1 and 2 ($p < .001$; Table 1.

unloading force versus displacement ($F - D_{ss}$) data set from a representative animal (TT01), along with the corresponding 1st-order linear regression models on the three test sites.

The equivalent compliance ($C_{eq,i}$) for each trial (i as trial index) was estimated by calculating the reciprocal of the average stiffness ($\overline{S}_i$) of the loading and unloading curves:

$$\overline{S}_i = \frac{1}{2}(k_L + k_U) \tag{4}$$

$$C_{eq,i} = \frac{1}{\overline{S}} = \frac{2}{k_L + k_U} \tag{5}$$

Equivalent compliance (C_{eq}) of each test site represents the overall steady state response of the integument at the spot during the static step loading experiment, with smaller values corresponding to a stiffer response.

The average and standard deviation of equivalent compliance (C_{eq}) for the three test sites was calculated by taking all the trials at the same test site across all the animals.

For the cyclic loading trials, tissue displacement (D) along with the corresponding measured pressure differentials (ΔP) were recorded and segmented into individual cycles for the three peak pressure conditions. Data for each cycle (loading and unloading) were then normalized to 100 points representing equal intervals from 0% to 100% using the spline function in MATLAB (Natick, MA). Initial (D_o), peak (D_p), and final (D_f) deformation were identified for each cycle, along with the corresponding pressure differentials (ΔP). Mean displacement ($\overline{D}$) and mean pressure differential ($\Delta\overline{P}$) at each test site were calculated by averaging across all the normalized trials from all the animals. Average force versus displacement ($\overline{F} - \overline{D}$) curves were then established accordingly using the normalized data as well (Figure 6a).

Energy loss ($E_{cycle,i}$) by the integument during each cyclic loading trial was estimated by calculating the area of the corresponding hysteresis loop present in the force versus displacement ($F - D$) curve via MATLAB *trapz* function:

$$E_{cycle,i} = \int_{D_o}^{D_p} F_L dD - \int_{D_f}^{D_p} F_U dD \tag{6}$$

where i represents trial index, F_L and F_U are the forces during loading and unloading, and D is the corresponding displacement of the integument. D_o, D_p, and D_f correspond to the initial, peak, and final displacement measured during the trial. Force and displacement data for loading and unloading of each cycle were evaluated separately and the enclosed area by the two curves was then used to calculate the energy loss ($E_{cycle,i}$) during the cycle (Nordin & Frankel, 2001). Mean and standard deviation of energy loss (E_{cycle}) were then calculated for each test site (Figure 6c).

Creep and recovery are time-dependent behaviors of viscoelastic material characterized by progressive material deformation under constant stress (Lakes, 2009). Integument response during the creep-recovery loading was modeled as exponential function and parameterized using the settling time required to reach 95% of the steady state displacement value during both loading (t_c) and unloading (t_r):

$$D = a + be^{-ct} \tag{7}$$

$$t_c = t_r = -\ln(0.05)/c \tag{8}$$

where D represents integument displacement, a, b, and c are the coefficients of the modeled exponential creep and recovery response.

To statistically compare the viscoelastic material properties among the three test sites, we performed the two-sample t test to quantify the statistical difference of equivalent compliance (C_{eq}), energy loss (E_{cycle}), and settling time (t_c, t_r) from static step, cyclic, and creep-recovery experiments, respectively. The significance level was set at 0.05, with $p > .05$ indicating lack of statistical significance, while $p \in [.01, .05]$, $p \in [.001, .01]$, and $p < .001$ identified as significant (*), highly significant (**), and very highly significant (***). The t-test results are presented in Table 1 and Figures 5(e), 6(c), and 7(c).

2.3.2 | Suction cup analysis

Suction cup shape (contact angle [θ_c], height [H_{sc}]) and attachment force (F_A) were used to characterize performance on both rigid and compliant substrates. Cup geometry was divided into two parts (Figure 4b): (1) Bell: from the lip at the substrate to the concave notch of the profile and (2) Neck: from the concave notch to the top of the suction cup which is enclosed inside the connection with the testing machine. Video data were used to parameterize deformation of the cup via extracting contact angle (θ_c) and suction cup height (H_{sc}) at each configuration during loading.

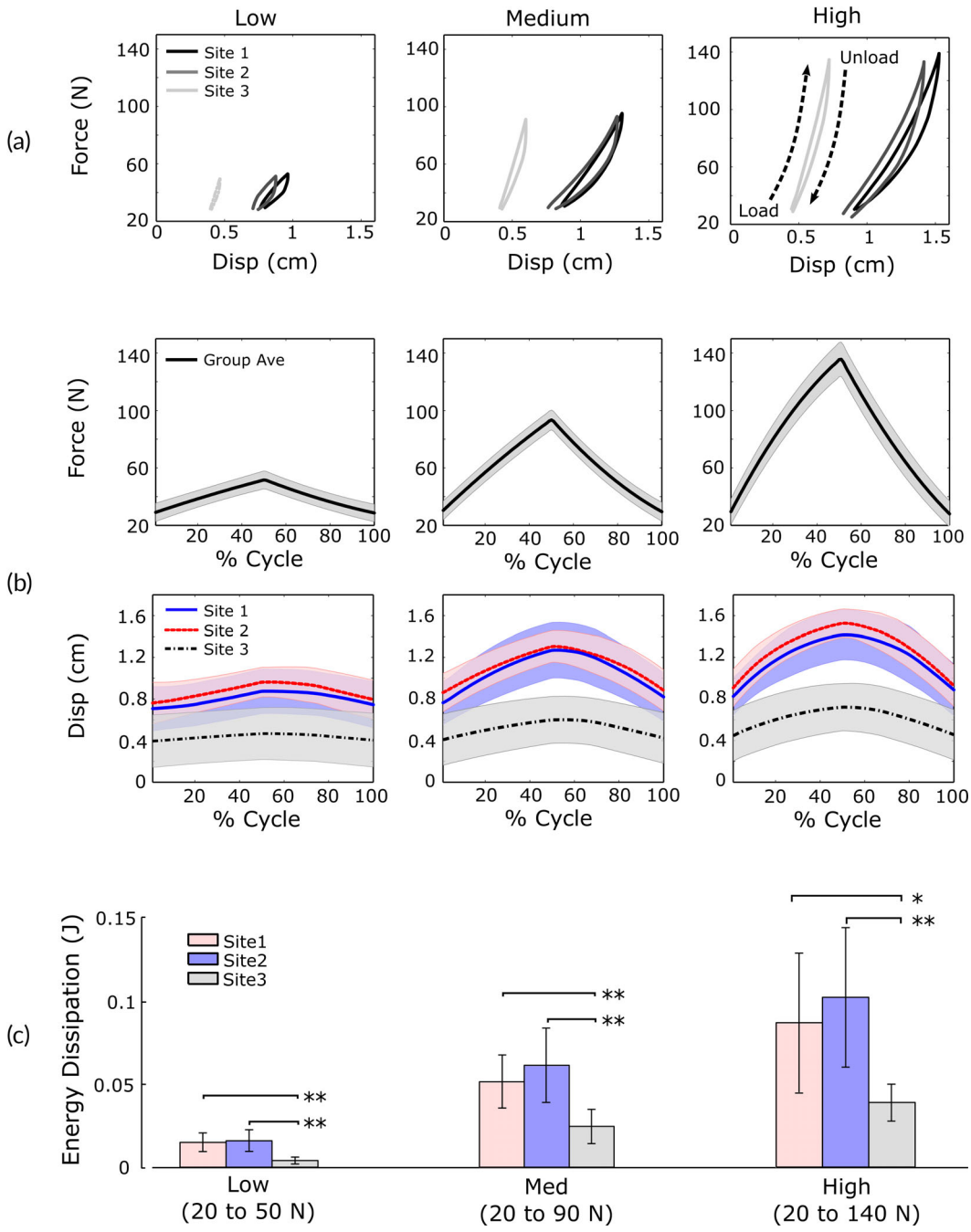


FIGURE 6 (a) Average force vs. displacement curves for the three sites during low, medium, and high-level cyclic loading. (b) The average cyclic force (black line) applied during the loading/unloading cycle are shown with one standard deviation around the average (gray shading). The average displacement (blue, red, and black dot-dashed lines) for each site and loading condition are also plotted with one standard deviation around the average. (c) Mean and standard deviation of the energy dissipation (E_{cycle}) at the three sites calculated using the area of the hysteresis loop for each loading condition and site. The results of *t* tests indicate either a highly significant (**) difference or a significant difference (*) between Site 3 and the other two sites while there is a lack of statistical significance between Sites 1 and 2 (Table 1).

TABLE 1 Statistical test results for viscoelastic material properties. The two-sample *t* test was performed to quantify difference between test sites for equivalent compliance (C_{eq}), energy loss (E_{cycle}), and settling time (t_c, t_r).

Static step loading			C_{eq}
Site 1–Site 2			0.371 NS
Site 1–Site 3			<0.001***
Site 2–Site 3			<0.001***
	E_{cycle}		
Cyclic loading	**Low**	**Medium**	**High**
Site 1–Site 2	0.782 NS	0.562 NS	0.219 NS
Site 1–Site 3	0.001**	0.005**	0.02*
Site 2–Site 3	0.002**	0.007**	0.0002**
Creep-recovery loading	**t_c (s)**		**t_r (s)**
Site 1–Site 2	0.04*		0.140 NS
Site 1–Site 3	0.754 NS		0.731 NS
Site 2–Site 3	0.03*		0.400 NS

NS $p > .05$.
*$p \in [.01, .05]$.
**$p \in [.001, .01]$.
***$p < .001$.

Contact angle (θ_c) was defined as the angle between the bottom edge of the lip and the tangential line of the bell, and the height of the suction cup (H_{sc}) was measured from the lip to the top of the cup, Figure 4(b).

In addition to geometry, attachment force (F_A) is another critical parameter to evaluate suction cup performance. The projected area under the cup was divided into two parts, the central circular area exposed to vacuum (vacuum area, A_v) and the area of the ring of material in contact with the substrate (contact area, A_c) (Ge et al., 2015; Figure 4b). In this study, limited by the ability to distinguish the two in camera footage, vacuum area:

$$A_V = \frac{\pi \cdot D_{lip}^2}{4} \tag{9}$$

was estimated using the measured cup diameter (D_{lip}, Figure 4b) from images taken during loading.

At initial setup, the normal components ($\hat{j}$ direction) of the attachment force (F_A), the normal force (N), and the resistive force (f') tangent to the contact between the cup lip and the substrate are balanced as shown in Figure 1. The force due to the resistive force (f') and atmospheric pressure (p_o) acting on the lip of the cup are both assumed to be negligible. As such, the attachment force (F_A) is equivalent to the vacuum force (F_V) created by the cup:

$$F_A = F_V = \Delta P \cdot A_v \tag{10}$$

Followed by the loading with a constant translational rate of 60 mm/min, the applied force (F_p) was assumed to equal the difference between the attachment force (F_A) and the normal force (N).

$$F_P = F_A - N \tag{11}$$

where F_p is the magnitude of the applied load from the universal tester. The vertical component ($\hat{j}$ direction) of the normal force (N) was then estimated as:

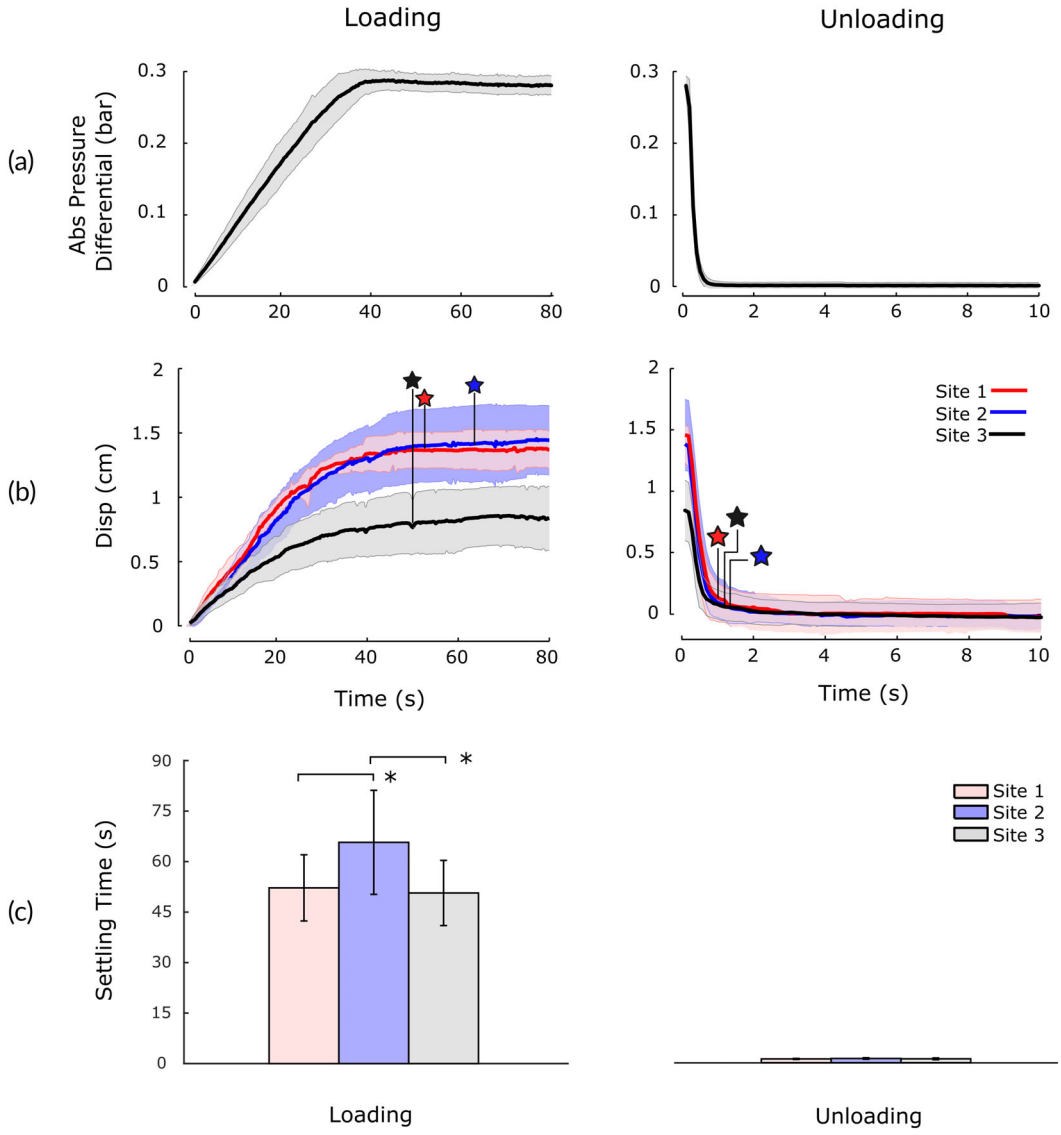


FIGURE 7 (a) Mean and standard deviation of absolute differential pressure ($|\Delta P|$, bar = 100 kPa) for creep and recovery loading at the three sites. (b) Mean and standard deviation of the resulting displacement at the three sites. The stars identify the average settling time, i.e., when the displacement attains 95% of the steady state value for each site during the loading and unloading phases. (c) Settling time compared across the three sites during loading (creep, t_c, left) and unloading (recovery, t_r, right), with the corresponding standard deviation bars. *T*-test results indicate a significant (*) difference between Site 2 and the other two sites for settling time during creep (t_c), Table 1.

$$N = \Delta P \cdot A_v - F_p \tag{12}$$

In our experiments, ΔP, A_v, and F_p were all measured. Via studying how the applied force (F_p), attachment force ($F_A = F_V$), and the normal force (N) fluctuate during trials, we evaluated suction cup performance on two substrates: a rigid acrylic sheet and the 00–10 silicone integument phantom. Force, pressure, and image data, collected during trials with the rigid and compliant substrates, were used to characterize cup performance starting at initial setup and

continuing to failure under normal loading. Data were then normalized to percentage of the trial (%Trial) using the time the loading was initiated (0%) to the time at failure (100%).

In addition to suction cup kinetics (F_p vs. $F_A = F_V$ vs. N), we conducted analysis to gain further insight into cup performance on a compliant substrate. First, the stiffness of the compliant substrate was calculated using experimental data and compared to the measured dolphin integument stiffness. Peak displacement of the substrate (D_p, Figure 4b) was defined as the maximum distance between the loaded substrate profile (H_s) and the initial setup height, which was calculated from video data. Measurements of displacement (D_p) and the applied load (F_p) were used to calculate substrate stiffness. Second, how the pressure differential (ΔP) and vacuum area (A_v) evolve during the loading was investigated. To do so, the normalized vacuum area ($\overline{A}_V$) was calculated by dividing the vacuum area estimated during the trial (A_v) by the area of the undeformed cup ($A_{V_{neutral}}$) and correlated with the corresponding absolute pressure differential ($|\Delta P|$). The $\overline{A}_V$ versus $|\Delta P|$ relationship was then used to compare how suction cup performance (attachment force [F_A], which equals to vacuum force [F_v]) was related to the deformation of the cup bell (internal volume V_{int} in Figure 1).

3 | RESULTS

3.1 | Integument testing results

3.1.1 | Static step loading

Figure 5 presents representative and group results from force versus displacement (F vs. D_{ss}) data collected from 11 animals. 1st-order linear regression was used to model the integument responses during loading and unloading at the three test sites. Representative data for an individual animal are presented in Figure 5(a) (loading) and (b) (unloading). Take Site 1 for example, the coefficients of the 1st-order term from the fit to these data ($k_{\overline{L}}^{1} = 78.1$, $k_{\overline{U}}^{1} = 100.00$) were used to calculate the equivalent compliance ($C_{eq,i} = 0.112$ mm/N) for this specific trial (i as trial index) using Equations 4 and 5. Average equivalent compliance for the three sites were 0.117, 0.108, and 0.060 mm/N at Sites 1, 2, and 3, respectively (Table 2, Figure 5e). Equivalent compliance at Site 3 was very highly statistically different than at Sites 1 and 2 ($p < .001$), while there is lack of statistical significance between Sites 1 and 2. Figure 5(c) presents the average force versus displacement curves ($\overline{F}$ vs. $\overline{D}_{ss}$) for the static step loading trials. A nonlinear stiffness response was observed at all three sites, with Site 3 having the stiffest response and the least hysteresis. At the highest loading condition (136 N) the integument displacement was twice as large at Sites 1 and 2 than at Site 3 (~1.5 cm vs. ~0.75 cm; Figure 5d). Statistical significance is reported in Table 1.

3.1.2 | Cyclic Loading

Figure 6(b) presents the average loading force and average integument displacement during the cyclic loading trials. Average force and displacement ($\overline{F}$ vs. $\overline{D}$) were used to plot hysteresis loops during the cyclic loading at the three levels, Figure 6(a). Once again, the integument at Site 3 was found to have the stiffest response with maximum displacement of around 0.7 cm at a peak load of ~135 N. The hysteresis loops at Sites 1 and 2 were comparable and had approximated maximum displacement of around 1.4 cm at peak loading. Nonlinear stiffening was present at all three sites during the loading phase of the cycle indicating that the stiffness of the integument increases at larger deformations. The energy loss (E_{cycle}) during the cyclic loading was comparable at Site 1 and 2, and much larger than the values calculated at Site 3, Table 2. For example, at the low-level loading condition, energy loss (E_{cycle}) at Site 1 (0.015 J) and 2 (0.016 J) are roughly four times of Site 3 (0.004 J).

TABLE 2 SSCup in vivo measurement results. The equivalent compliance (C_{eq}) represents the displacement (mm) of the substrate per unit loading (*N*), a larger C_{eq} means the integument at the site deforms more under the same loading. Energy loss (E_{cycle} [J]) is the magnitude of energy dissipated by the integument during the cyclic loading. A larger E_{cycle} results from a larger hysteresis loop (energy difference) between the loading and unloading curve. Settling time for creep (t_c [s]) and recovery (t_r [s]) indicates the time taken by the integument at the three sites to reach 95% of steady state displacement during loading and unloading.

Static step loading		Cyclic loading E_{cycle} (J)			Creep-recovery loading	
Test site	C_{eq} (mm/N)	Low	Medium	High	t_c (s)	t_r (s)
Site 1	0.117 ± 0.021	0.015 ± 0.006	0.051 ± 0.016	0.087 ± 0.042	52.21 ± 9.83	1.11 ± 0.15
Site 2	0.108 ± 0/021	0.016 ± 0.007	0.061 ± 0.022	0.102 ± 0.042	65.73 ± 15.45	1.25 ± 0.22
Site 3	0.060 ± 0.019	0.004 ± 0.002	0.024 ± 0.010	0.039 ± 0.011	50.69 ± 9.68	1.15 ± 0.27

3.1.3 | Creep-recovery loading

Results from the creep-recovery trials were used to characterize the temporal response of the integument under loading (Figure 7, Tables 1 and 2). During creep section, the maximum pressure differential (0.3 bar = 30 kPa) was reached 40 s after the initiation of the trial, and the integument at Site 3 had the fastest response with a creep settling time of 50.69 ± 9.68 s, Figure 7 (b, left). During recovery section, pressure was released from the chamber in <1 s. Sites 1, 2, and 3 had comparable recovery times of 1.11 ± 0.15 s, 1.25 ± 0.22 s, and 1.15 ± 0.27 s (Figure 7 (b, right), without significant difference based on statistical analysis results, Figure 7(c).

3.2 | Suction cup testing results

3.2.1 | Suction cup kinematics

The deformation of the suction cups on the two substrates was visibly different. Figure 8 presents image data from 0%, 25%, 50%, 75%, and 100% of a representative trial with the (A) rigid and (B) compliant substrates. On the rigid substrate, the cup exhibited a two-stage deformation, with initial deformation at the neck followed by an elongation and expansion of the bell. Initially, cups on the rigid substrate had a flatter setup profile ($\theta_c = 30.45^\circ$; $H_{sc} = 20.46$ mm) compared to cups on the compliant substrate ($\theta_c = 48.92^\circ$; $H_{sc} = 23.13$ mm) (the 1st column of Figure 8). This was characterized by a smaller contact angle (θ_c) and a lower suction cup height (H_{sc}). During initial loading on the compliant substrate, there was little visible deformation of the neck. As loading increased the bell and substrate deformed together until failure. Deformation of the compliant substrate resulted in a smaller cup diameter (D_{lip}) with a more pronounced concave shape when first attached. During loading the cup and substrate deformation were coupled. The substrate deformed into the cup and reduced the internal volume (V_{int}) throughout the loading, leading to a lower internal pressure (p_v) and smaller pressure differential (ΔP). Just before failure, cups on both substrates had similar vacuum areas:

$$A_V \cong \frac{\pi \cdot D_{lip}^2}{4}, \tag{13}$$

Figure 8 (5th column) and Figure 9(b). But the cup on the rigid substrate had a larger contact angle ($\theta_c = 68.78^\circ$) and a higher suction cup height ($H_{sc} = 26.87$), leading to a larger internal volume (V_{int}) compared to cups on the

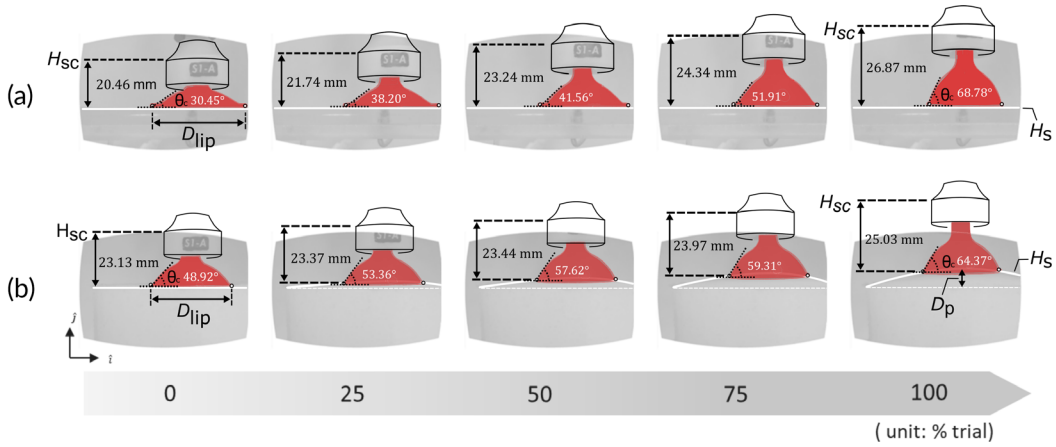


FIGURE 8 Suction cup deformation during normal loading on (a) a rigid (acrylic) substrate and (b) a compliant (00–10) substrate. There are noticeable differences in the overall cup deformation (contact angle [θ_c], height [H_{sc}]) between the two cases, which in turn influences cavity expansion (internal volume [V_{int}], vacuum area [A_v]) and cups performances ($F_A = F_V$).

compliant substrate ($\theta_c = 64.37°$, $H_{sc} = 25.03$). These changes in geometry result in a larger internal volume (V_{int}), a lower internal pressure (p_v), and therefore larger vacuum force ($F_V = F_A$) for cups on a rigid substrate. The stiffness of the compliant substrate compares well to the measured integument compliance at Sites 1 and 2 from the SSCup dolphin experiment (Figure 9a).

3.2.2 | Suction cup kinetics

When first attached, the magnitude of the vacuum force (F_V) generated by the cup and the normal force (N) are equal and opposite (Equation 9). At this point the cup is in compression and the normal force created by the deformation of the cup is acting to restore the cup to its initial shape. The average initial vacuum force (F_V) was slightly larger for cups attached to the rigid substrate (~25 N vs. 23 N; Figure 10). As the applied load (F_p) increases, the magnitude of the vacuum force (F_V) also increases, while the normal force (N) decreases as the shape of the cup approaches its undeformed state. Figure 10 (top) presents the silhouettes that capture the deformation of the cups at 0%, 25%, 50%, 75%, and 100% of the trial, along with a vector estimating the magnitude and direction of the corresponding normal force (N).

The cups on both substrates were loaded with a constant displacement of 60 mm/min, but the average applied force ($F_{p,avg}$) at failure was twice as large for cups tested on the rigid substrate (50 N vs. 25 N). On the rigid substrate, the cups had two distinct regions of roughly linear stiffness: a lower stiffness from 0% to 20% of the trial, and then a higher stiffness up to failure (Figure 10a). The stiffness response of the cups tested on the compliant substrate was closer to linear throughout the entire trial (Figure 10b). On the rigid substrate, the cup deformed more than that on the compliant substrate, transitioning from compression to tension at ~86% of the trial. On the compliant substrate, the suction cup and the substrate both deform during loading but fail before the transition from compression to tension. In both cases, cup deformation created by the applied force (F_p) increases the cup internal volume (V_{int}), decreases the pressure differential (ΔP), while increases the absolute value ($|\Delta P|$), and increases the vacuum force (F_V). This continues until a leakage pathway at the lip of the cup results in attachment failure. Cups tested on the rigid substrate deformed more and failed at larger applied forces (F_p).

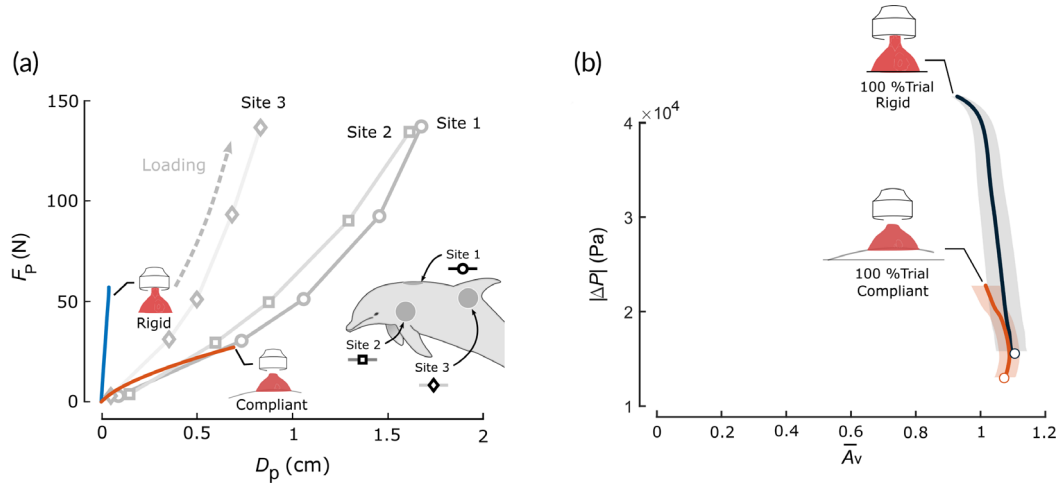


FIGURE 9 (a) Force (F_p) versus peak displacement (D_p) during the SSCup static step loading (gray lines and points) is compared to data collected from the substrates during the suction cup testing. The stiffness of the compliant (00–10) substrate compares well to the values measured at Sites 1 and 2. (b) Correlation between the normalized vacuum area ($\overline{A}_V = A_V/A_{V_{neutral}}$) and the absolute pressure differential ($|\Delta P|$).

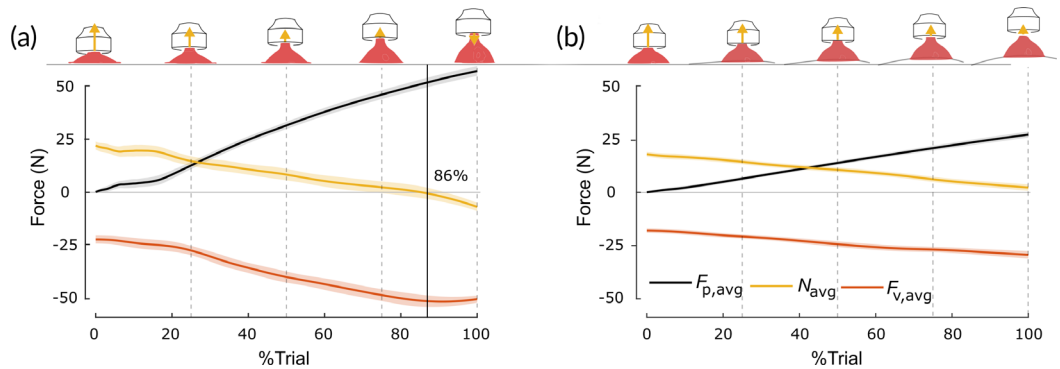


FIGURE 10 A comparison of the average cup performance during normal loading on (a) rigid and (b) compliant substrates. The average pulling force (F_P), normal force (N_{avg}), and vacuum force ($F_{V,avg} = F_{A,avg}$) are shown for each substrate, with the shaded area represents one standard deviation from the average value. The direction and magnitude of the average normal force (N_{avg}) is illustrated with arrows in the silhouettes of the cups on the top of each plot.

4 | DISCUSSION

Despite the widespread use of suction cups to attach biologging tags to cetaceans, little is known about the factors that control the tenacity of this attachment method. Compared to the rigid substrates on which suction cups are typically used, cetacean integument is viscoelastic, raising the questions of how integument compliance affects cup mechanics and whether cups can be designed to improve performance on a compliant substrate. This study makes a first step to address these questions. Specifically, we used an experimental approach to (1) characterize dolphin integument mechanics at typical tag attachment sites and (2) compare cup performance on compliant and rigid substrates. Measurements of integument deformation under vacuum loading were made at three sites on common bottlenose dolphins using a novel in vivo measurement system, SSCup. Integument deformation at all three sites

demonstrated a viscoelastic response, but the fibrous tissue around the dorsal fin (Site 3) differed greatly from the other two sites on the trunk. Site 3 had roughly half the equivalent compliance (C_{eq}), less than half the energy loss (E_{cycle}) when vacuum loading was cycled and approximately half the average peak displacement ($\overline{D}_p$) compared to the sites on the trunk (Site 1 and 2; Table 2, Figures 5D and 6B).

The same pressure loading range (5–30 kPa) was applied to dolphin integument with different frequencies during the static step and high-level cyclic loading trials (Figure 3b). The three test sites responded similarly under the two loading profiles, with average peak displacements ($\overline{D}_p$) around 0.7 cm for Site 3, and 1.5 cm for Sites 1 and 2. Nevertheless, it is also found that the peak displacement (D_p) at the site with highest stiffness (Site 3) was less sensitive to loading frequency. While the more compliant sites (Site 1 and 2), each with a time-dependent viscoelastic response, had slightly larger average peak displacements ($\overline{D}_p \geq 1.5$ mm; Figure 5c) during the static step trials compared to the cyclic loading trials ($\overline{D}_p \geq 1.5$ mm; Figure 6a,b, 3rd column). These results indicate that the frequency of hydrodynamic loading created by drag forces acting on a tag could impact the response of the integument at the attachment site.

Differences in viscoelastic response demonstrate the inhomogeneity of cetacean integument created by distinct anatomical substructures, including varying amounts of subdermal fat, bone, and muscle underneath each test site. CT scans (Figure 2a) show how suction cups deform integument at the three sites examined in this work. However, because these images are from a cadaver, they will not reflect the same magnitude of deformation expected from living swimming animals. Suction cup shape (contact angle [θ_c] and height [H_{sc}]) and attachment force (F_A) were used to characterize performance on both rigid and compliant substrates. The deformation observed on compliant substrate reduces the internal volume (V_{int}) of the cup, leading to smaller pressure differentials (ΔP) when compared to measurements made with the same cups on a rigid substrate (Figure 1).

To investigate the impact of substrate compliance on cup performance, silicone suction cups were attached to both rigid (acrylic) and compliant (Shore A 00–10 silicone rubber) surfaces and loaded to failure (detachment). The load-deformation response of these two engineered materials brackets measured compliances at the three test sites on the dolphins (Figure 9a). As such, suction cup performance on a dolphin might be expected to fall between the results measured on these two substrates. Material response is dependent on strain rate (Lakes, 2009), and the low displacement rate (60 mm/min) used for the tests is more likely to represent relatively slow hydrodynamic force changes experienced by a suction cup attached to a marine animal traveling at a steady speed. The cup and substrate act as a coupled system affecting both the initial setup pressure and the cup's response to loading. When unloaded, the deformation of the compliant surface merges into the cup leads to a lower vacuum force (F_V) and different mechanics at the lip-substrate interface as compared to a cup on a rigid substrate (Figures 1 and 8). During loading on the compliant substrate, both the cup and substrate deform together until a leakage path is created at the lip, resulting in failure (Figure 8).

Our experimental results demonstrate that cup performance is significantly impacted by a compliant substrate. Peak applied force (F_p) at failure on the compliant substrate (~25 N) was half of the value on the rigid substrate (~50 N). Prior to failure, suction cups attached to the rigid substrate generated absolute pressure differentials ($|\Delta P|$) that were more than twice as large as cups attached to the compliant one even though the projected cup area at failure was comparable (Figure 9b). Thus, the tenacity of suction cups may depend strongly on the stiffness of the integument at the attachment site. This, in turn, depends on the anatomy of the underlying tissues at the site: areas of the body such as cranial to the dorsal fin anterior insertion, where there is more fibrous tissue and less blubber or muscle, tend to have lower compliance, which may result in improved cup performance during hydrodynamic loading. Furthermore, the level of physical activity and associated musculoskeletal movement, as well as the skin tension during locomotion may also contribute to the material properties of the integument and the overall attachment performance of suction cups as well.

During a deployment, the forces that a cup needs to resist for tag attachment are directly related to the movement kinematics of the animal. Animals swim at a range of speeds creating hydrodynamic loads on the tag in both normal (lift force) and shear (drag force) directions. Loading magnitude will depend on the speed of the animal.

Steady state dolphin swimming speeds ranging from 1 to 5 m/s measured with tags (Gabaldon et al., 2022) can create drag forces ranging from 1 to 15 N and lift forces ranging from 1 to 60 N on a tag 150 mm long with a maximum frontal cross-sectional area of 2,200 mm^2 (Shorter et al., 2014). The experimentally measured lift force at 5 m/s from this example tag exceeds the failure force of a single cup on a compliant substrate (60 N vs. 25 N), but biologging tags tend to be secured to an animal using an array of four cups. If the performances of the cups scale linearly, an array of four cups would require an applied normal load greater than ~100 N before failure. Forces of these magnitudes could be generated by the flow around the tags during high-speed swimming (>6 m/s), during large accelerations/decelerations while the animals swim and maneuver, or from impacts between the tag and the environment or other animals. In the event that one or more cups fail, smaller hydrodynamic forces would result in tag detachment. In addition to having the stiffest response to the loading among the three test sites, Site 3 is located near the COM (center of mass), which could potentially reduce the effect of body motion that occurs during locomotion.

The high-pressure differentials generated by a suction cup during fast swimming impose local stresses on the integument. Figure 9(b) shows that the cup absolute pressure differential ($|\Delta P|$) on the compliant substrate reached ~20 kPa at failure. Understanding if the stress generated by peak loading of this magnitude is large enough to damage integument at the attachment site is an important consideration for cup design. Cupping, a form of myofascial massage therapy where local suction is used to draw fluid from tissue and muscle to the skin surface, loads human integument in a comparable manner to the SSCup. In a numerical study of cupping mechanics, Tham et al. (2006) illustrated that normal stress generated using a rigid dome result in both tensile and compressive stress on the integument. In the simulations, compressive stress was highest directly below the cup rim, and the largest tensile forces were generated just inside the rim and at the center of the cup. These tensile stresses cause capillary dilation resulting in the movement of interstitial fluid to the integument surface, and if the tensile stress is large enough, the capillaries could rupture. Pressure differentials (ΔP) of up to 30 kPa (0.3 bar) were used to load the dolphin integument with the SSCup. Following the testing the tissue was observed to be raised, and the surface temperature had increased at the attachment site (Figure 11) but no discoloration was observed. A portable ultrasound unit was used opportunistically to image the integument after loading, and no fluid pooling was visible in the images. The peak absolute pressure differentials ($|\Delta P|$) measured during cup failure testing (~40 kPa on the rigid substrate and ~ 20 kPa on the compliant substrate, Figure 9b) and during the experimental investigation of integument mechanics with the SSCup (30 kPa) are comparable, but the resulting force applied to the integument by the SSCup (~140 N) was significantly higher than the cup on either substrate (~50 N on the rigid substrate and ~ 25 N on the compliant substrate) due to the larger area ($A_S = 45.6\ cm^2$) of the SScup compared to the suction cups ($A_{neutral} = 15.9\ cm^2$). Importantly, the tensile stresses that can lead to capillary rupture will be reduced for smaller projected areas at the same relative pressure differential ($p_o - p_v$). In simulation, Tham et al. (2006) predicted that peak stress would decrease from ~32 kPa to ~18 kPa when the diameter of the cup was decreased from 65 to 35 mm for the same 30 kPa pressure differential (ΔP). These results indicate that the stress acting on the integument can be modulated by controlling the size of the cup and the magnitude of the pressure differential (ΔP) generated during attachment.

Diving behavior will also result in cyclic changes to the pressure differential (ΔP) between the cup and environment, and therefore the attachment force (F_A). Cups are placed on the animals at the surface in atmospheric pressure (p_{atm}). During a dive, the environmental pressure (p_o) surrounding the cup and animal will grow, resulting in a larger relative pressure differential ($p_o - p_v$) than at the surface. The forces created by these pressure differentials (ΔP) will deform the cup, modifying the internal volume (V_{int}) and the projected area (A_v, A_c). This results in coupled dynamics that affect the suction cup attachment force (F_A): specifically, the pressure differential (ΔP) will increase, but the projected area of the cup (A_v, A_c) is expected to decrease as the animal dives. These dynamics will also affect the stress on the integument with the larger stresses created by the increased pressure differential being offset by a smaller effective cup area. However, the tissue loading induced by suction cups as a function of dive depth has yet to be measured in situ and it remains uncertain whether the risk of damage to the integument increases as animals dive.

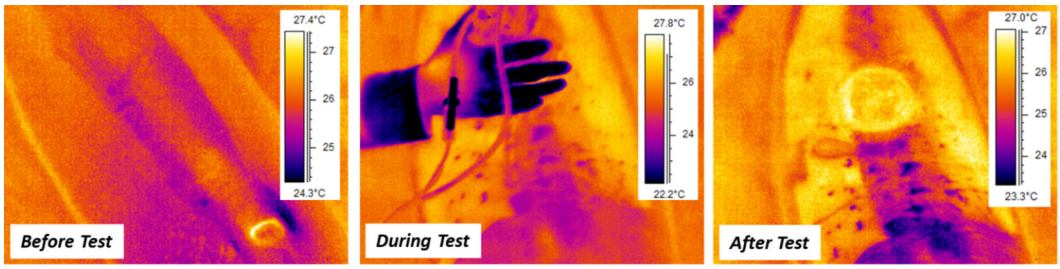


FIGURE 11 Thermal images of Test Site 1 before, during, and after a static step loading trial. After the trial was completed, there was a visible impression corresponding to the footprint of the SSCup with an elevated local temperature, but there was no visual damage or discoloration to the integument following the testing.

Although the potential for suction cups to cause harmful levels of stress in the integument under normal loading conditions is unclear, there are several practical ways to reduce the skin load and therefore the risk of harm. The attachment force ($F_A = A_V$) generated by a cup is determined by the projected vacuum area (A_v) and the pressure differential (ΔP) between the cup volume (p_v) and the environment (p_o). The compliance of a suction cup influences both the pressure differential (ΔP) and the interaction with the substrate. Cup compliance depends on both shape and material: compliance can be increased be selecting a softer material for a given cup geometry, or by reducing the thickness of the cup walls. For a given cup geometry, e.g., the same projected vacuum area (A_v), a more compliant cup will generate a lower pressure differential (ΔP), resulting in lower tissue stress but also a lower attachment force (F_A). The magnitude of the attachment force (F_A) could be maintained by increasing the size of the cup to grow the projected cup area. However, the pressure differential (ΔP) at cup failure would need to be quantified, because integument stress scales with the size of the projected area (A_v, A_c) of the cup for a given pressure differential (ΔP) (Tham et al., 2006). Additionally, a softer cup may have an increased risk of detachment by other mechanisms, e.g., buckling of the cup or folding of the lip during attachment. Further, if cups are used to attach movement sensors to an animal, compliant cups will deform more under cyclic hydrodynamic loading increasing noise in the sensor measurements. Future cup designs should also address leakage to improve performance. Leakage created by imperfections at the interface between the cup and animal will result in a reduction in the attachment force (F_A) during a deployment. Preliminary work is currently being conducted to investigate the performance of hybrid cups with a stiffer bell and a compliant lip. The use of materials with variable compliance could result in a more robust seal while still generating a desired pressure differential (ΔP).

In this study, we only investigated cup performance during normal loading, i.e., perpendicular to the integument surface, but the hydrodynamic forces acting on a biologging tag will generate both normal (lift) and shear (drag) forces. Additional testing to characterize performance during shear loading is needed to understand failure modes and improve tag/cup designs. The main force resisting shear loading can be approximated using friction models like Coulomb's law. For this model, the resistive force (f') is dependent on both the normal force (N) and the friction coefficient on the contact surface. For our case, the normal force (N) is positively related to the vacuum force (F_V) per Equation (12). A compliant integument reduces the vacuum force (F_V) but tends to increase the contact surface area (A_c) as the substrate deforms into the cup, Figure 1(b). The net impact of integument compliance on shear force resistance is therefore complex and will require improved integument surrogates for lab testing.

Biologging tags are attached with suction cups on an ever-increasing range of species. Our results suggest that animals with thicker, less fibrous blubber will tend to have more compliant integument leading to greater deformations at the skin surface for a given cup stiffness. To minimize tissue strain, larger cups with lower pressure differential (i.e., softer cups) should be selected for use on animals with more compliant integument. As integument properties can vary with ontogeny, body condition, and habitat even within a species, measurements from more animals and from multiple locations will be important to inform the design and selection of cups for biologging tags.

However, in vivo measurements of animals in good condition are seldom possible for many species, especially larger whales. In these situations, using ex vivo samples and simplified proxies for integument mechanics, e.g., indentation hardness tests or tensile tests (Grear et al., 2018) could provide initial context and perspective about the attachment surface.

ACKNOWLEDGMENTS

The authors acknowledge Tom Hurst for all his help with the instrument design and data collection, Darlene Ketten and Julie Arruda for CT scanning support, and the trainers and the animals at Dolphin Quest Oahu. We are grateful for the efforts of the staff, students, veterinarians, collaborators, and handlers of the Chicago Zoological Society's Sarasota Dolphin Research Program for safely and effectively providing access to wild dolphins during health assessment operations.

AUTHOR CONTRIBUTIONS

Ya-Yu Yang: Conceptualization; data curation; investigation; methodology; resources; software; visualization; writing – original draft; writing – review and editing. **K. Alex Shorter:** Conceptualization; data curation; formal analysis; funding acquisition; investigation; methodology; project administration; resources; software; visualization; writing – original draft; writing – review and editing. **Michael Moore:** Conceptualization; funding acquisition; investigation; writing – original draft; writing – review and editing. **Julie Rocho-Levine:** Investigation; writing – original draft; writing – review and editing. **Randall Wells:** Investigation; writing – original draft; writing – review and editing. **Kira Barton:** Formal analysis; visualization; writing – original draft; writing – review and editing. **Mark Johnson:** Conceptualization; funding acquisition; methodology; project administration; supervision; writing – original draft; writing – review and editing.

FUNDING

This project was funded by the National Oceanographic Partnership Program (National Science Foundation via the Office of Naval Research, N00014-11-1-0113). Dolphin Quest, Inc. funded the health assessment operations in Sarasota Bay and provided in kind support and behavioral training for the experimental measurements. Support for analysis was provided by the Canadian Department of Fisheries and Oceans (DFO).

ORCID

K. Alex Shorter https://orcid.org/0000-0003-3825-8210
Randall S. Wells https://orcid.org/0000-0001-9793-4181

REFERENCES

Aslam, D. M., & Dangi, G. D. (2005). Design, fabrication and testing of a smart robotic foot. *Robotics and Autonomous Systems*, *51*(2–3), 207–214. https://doi.org/10.1016/j.robot.2004.09.019

Bahr, B., Li, Y., & Najafi, M. (1996). Design and suction cup analysis of a wall climbing robot. *Computers & Electrical Engineering*, *22*(3), 193–209. https://doi.org/10.1016/0045-7906(95)00039-9

Bercoff, J., Tanter, M., & Fink, M. (2004). Supersonic shear imaging: a new technique for soft tissue elasticity mapping. *IEEE Transactions on Ultrasonics, Ferroelectrics, and Frequency Control*, *51*(4), 396–409. https://doi.org/10.1109/TUFFC.2004.1295425

Cua, A. B., Wilhelm, K. P., & Maibach, H. I. (1990). Elastic properties of human skin: relation to age, sex, and anatomical region. *Archives of Dermatological Research*, *282*, 283–288.

Diridollou, S., Patat, F., Gens, F., Vaillant, L., Black, D., Lagarde, J. M., Gall, Y., & Berson, M. (2000). In vivo model of the mechanical properties of the human skin under suction. *Skin Research and Technology*, *6*(4), 214–221. https://doi.org/10.1034/j.1600-0846.2000.006004214.x

Elsner, P., Wilhelm, D., & Maibach, H. I. (1990). Mechanical properties of human forearm and vulvar skin. *British Journal of Dermatology*, *122*(5), 607–614. https://doi.org/10.1111/j.1365-2133.1990.tb07282.x

Escoffier, C., de Rigal, J., Rochefort, A., Vasselet, R., Lévêque, J. L., & Agache, P. G. (1989). Age-related mechanical properties of human skin: an in vivo study. *Journal of Investigative Dermatology*, *93*(3), 353–357. https://doi.org/10.1016/0022-202X(89)90058-4

Evans, S. L., & Holt, C. A. (2009). Measuring the mechanical properties of human skin *in vivo* using digital image correlation and finite element modelling. *Journal of Strain Analysis for Engineering Design*, *44*(5), 337–345. https://doi.org/10.1243/03093247JSA488

Fish, F. E., & Rohr, J. (1999). *Review of dolphin hydrodynamics and swimming performance* (Technical Report 1801). SPAWARS System Center, San Diego, CA.

Fitzgerald, E. R., & Fitzgerald, J. W. (1995). Blubber and compliant coatings for drag reduction in water I. Viscoelastic properties of blubber and compliant coating materials. *Materials Science and Engineering: C*, *2*(4), 209–214. https://doi.org/10.1016/0928-4931(95)00079-8

Gabaldon, J. T., Zhang, D., Rocho-Levine, J., Moore, M. J., Van der Hoop, J., Barton, K., & Shorter, K. A. (2022). Tag-based estimates of bottlenose dolphin swimming behavior and energetics. *Journal of Experimental Biology*, *225*(22), jeb244599. https://doi.org/10.1242/jeb.244599

Ge, D., Matsuno, T., Sun, Y., Ren, C., Tang, Y., & Ma, S. (2015). Quantitative study on the attachment and detachment of a passive suction cup. *Vacuum*, *116*, 13–20. https://doi.org/10.1016/j.vacuum.2015.02.013

Grear, M. E., Motley, M. R., Crofts, S. B., Witt, A. E., Summers, A. P., & Ditsche, P. (2018). Mechanical properties of harbor seal skin and blubber—a test of anisotropy. *Zoology*, *126*, 137–144. https://doi.org/10.1016/j.zool.2017.11.002

Hanson, M. B., & Baird, R. W. (1998). Dall's porpoise reactions to tagging attempts using a remotely-deployed suction-cup tag. *Marine Technology Society Journal*, *32*(2), 18–23.

Hendriks, F. M., Brokken, D., Oomens, C. W. J., Bader, D. L., & Baaijens, F. P. T. (2006). The relative contributions of different skin layers to the mechanical behavior of human skin in vivo using suction experiments. *Medical Engineering & Physics*, *28*(3), 259–266. https://doi.org/10.1016/j.medengphy.2005.07.001

Hooker, S. K., & Baird, R. W. (2001). Diving and ranging behavior of odontocetes: a methodological review and critique. *Mammal Review*, *31*(1), 81–105. https://doi.org/10.1046/j.1365-2907.2001.00080.x

Horning, M., Andrews, R. D., Bishop, A. M., Boveng, P. L., Costa, D. P., Crocker, D. E., Haulena, M., Hindell, M., Hindle, A. G., Holser, R. R., Hooker, S. K., Hückstädt, L. A., Johnson, S., Lea, M., McDonald, B. I., McMahon, C. R., Robinson, P. W., Sattler, R. L., Shuert, C. R., … & Womble, J. N. (2019). Best practice recommendations for the use of external telemetry devices on pinnipeds. *Animal Biotelemetry*, *7*(1), 1–17. https://doi.org/10.1109/JOE.2002.808212

Isojunno, S., Aoki, K., Curé, C., Kvadsheim, P. H., & Miller, P. J. O. M. (2018). Breathing patterns indicate cost of exercise during diving and response to experimental sound exposures in long-finned pilot whales. *Frontiers in physiology*, *9*, Article 408459. https://doi.org/10.3389/fphys.2018.01462

Johnson, M. P., & Tyack, P. L. (2003). A digital acoustic recording tag for measuring the response of wild marine mammals to sound. *IEEE Journal of Oceanic Engineering*, *28*(1), 3–12. https://doi.org/10.1109/JOE.2002.808212

Kleivane, L., Kvadsheim, P. H., Bocconcelli, A., Øien, N., & Miller, P. J. (2022). Equipment to tag, track and collect biopsies from whales and dolphins: the ARTS, DFHorten and LKDart systems. *Animal Biotelemetry*, *10*(1), Article 32. https://doi.org/10.1186/s40317-022-00303-0

Kovacs, K. M., Thewissen, J. G., & Würsig, B. G. (Eds.) (2018). *Encyclopedia of marine mammals*. Academic Press

Lakes, R. S. (2009). *Viscoelastic materials*. Cambridge University Press.

Liu, J., Tanaka, K., Bao, L. M., & Yamaura, I. (2006). Analytical modelling of suction cups used for window-cleaning robots. *Vacuum*, *80*(6), 593–598. https://doi.org/10.1016/j.vacuum.2005.10.002

Mantriota, G., & Messina, A. (2011). Theoretical and experimental study of the performance of flat suction cups in the presence of tangential loads. *Mechanism and Machine Theory*, *46*(5), 607–617. https://doi.org/10.1016/j.mechmachtheory.2011.01.003

Miyake, T., Ishihara, H., & Tomino, T. (2009, February 22). Vacuum-based wet adhesion system for wall climbing robots-lubricating action and seal action by the liquid. *2008 IEEE International Conference on Robotics and Biomimetics* (pp. 1824–1829), Bangkok, Thailand. https://doi.org/10.1109/ROBIO.2009.4913279

Miyake, T., Ishihara, H., & Yoshimura, M. (2007, October 29). Basic studies on wet adhesion system for wall climbing robots. *2007 IEEE/RSJ International Conference on Intelligent Robots and Systems* (pp. 1920–1925), San Diego, CA. https://doi.org/10.1109/IROS.2007.4399417

Nachtigall, P. E. (2009). Glossary. In B. G. Würsig, J. G. Thewissen, & K. M. Kovacs (Eds.), *Encyclopedia of marine mammals* (pp. 1271–1294). Academic Press.

Nightingale, K., Soo, M. S., Nightingale, R., & Trahey, G. (2002). Acoustic radiation force impulse imaging: in vivo demonstration of clinical feasibility. *Ultrasound in Medicine & Biology*, *28*(2), 227–235. https://doi.org/10.1016/S0301-5629(01)00499-9

Nordin, M., & Frankel, V. H. (Eds.). (2001). *Basic biomechanics of the musculoskeletal system*. Lippincott Williams & Wilkins.

Özkaya, N., Leger, D., Goldsheyder, D., & Nordin, M. (Eds.) (2016). *Fundamentals of biomechanics: Equilibrium, motion, and deformation*. Springer.

Pabst, D. A. (1996a). Morphology of the subdermal connective tissue sheath of dolphins: a new fibre wound, thin walled, pressurized cylinder model for swimming vertebrates. *Journal of Zoology*, *238*(1), 35–52. https://doi.org/10.1111/j.1469-7998.1996.tb05378.x

Pabst, D. A. (1996b). Springs in swimming animals. *American Zoologist*, *36*(6), 723–735. https://doi.org/10.1093/icb/36.6.723

Pailler-Mattei, C., Bec, S., & Zahouani, H. (2008). In vivo measurements of the elastic mechanical properties of human skin by indentation tests. *Medical Engineering & Physics*, *30*(5), 599–606. https://doi.org/10.1016/j.medengphy.2007.06.011

Pavlov, V. V. (2006). Dolphin skin as a natural anisotropic compliant wall. *Bioinspiration & Biomimetics*, *1*(2), Article 31. https://doi.org/10.1088/1748-3182/1/2/001

Ratner, B. D., Hoffman, A. S., Schoen, F. J., & Lemons, J. E. (2004). *Biomaterials science: An introduction to materials in medicine*. Elsevier.

Rutkowski, M. M., Smolinski, P. J., & Miller, M. C. (2009). The geometry of vacuum assisted interface adhesion: Resistance to axial moment. *Vacuum*, *83*(5), 869–872. https://doi.org/10.1016/j.vacuum.2008.09.004

Sanders, R. (1973). Torsional elasticity of human skin in vivo. *Pflügers Archiv*, *342*, 255–260. https://doi.org/10.1007/BF00591373

Sandrin, L., Fourquet, B., Hasquenoph, J. M., Yon, S., Fournier, C., Mal, F., Christidis, C., Ziol, M., Poulet, B., Kazemi, F., Beaugrand, M., & Palau, R. (2003). Transient elastography: a new noninvasive method for assessment of hepatic fibrosis. *Ultrasound in Medicine & Biology*, *29*(12), 1705–1713. https://doi.org/10.1016/j.ultrasmedbio.2003.07.001

Schneider, K., Baird, R. W., Dawson, S., Visser, I., & Childerhouse, S. (1998). Reactions of bottlenose dolphins to tagging attempts using a remotely-deployed suction-cap tag. *Marine Mammal Science*, *14*(2), 316–324. https://doi.org/10.1111/j.1748-7692.1998.tb00720.x

Shorter, K. A., Murray, M. M., Johnson, M., Moore, M., & Howle, L. E. (2014). Drag of suction cup tags on swimming animals: modeling and measurement. *Marine Mammal Science*, *30*(2), 726–746. https://doi.org/10.1111/mms.12083

Solav, D., Moerman, K. M., Jaeger, A. M., Genovese, K., & Herr, H. M. (2018). MultiDIC: An open-source toolbox for multi-view 3D digital image correlation. *IEEE Access*, *6*, 30520–30535. https://doi.org/10.1109/ACCESS.2018.2843725

Takema, Y., Yorimoto, Y., Kawai, M., & Imokawa, G. (1994). Age related changes in the elastic properties and thickness of human facial skin. *British Journal of Dermatology*, *131*(5), 641–648. https://doi.org/10.1111/j.1365-2133.1994.tb04975.x

Tham, L. M., Lee, H. P., & Lu, C. (2006). Cupping: from a biomechanical perspective. *Journal of biomechanics*, *39*(12), 2183–2193. https://doi.org/10.1016/j.jbiomech.2005.06.027

Weickenmeier, J., Jabareen, M., & Mazza, E. (2015). Suction based mechanical characterization of superficial facial soft tissues. *Journal of Biomechanics*, *48*(16), 4279–4286. https://doi.org/10.1016/j.jbiomech.2015.10.039

Wells, R. S. (2009). Learning from nature: bottlenose dolphin care and husbandry. *Zoo Biology*, *28*(6), 635–651. https://doi.org/10.1002/zoo.20252

Wells, R. S., Rhinehart, H. L., Hansen, L. J., Sweeney, J. C., Townsend, F. I., Stone, R., Casper, D. R., Scott, M. D., Hohn, A. A., & Rowles, T. K. (2004). Bottlenose dolphins as marine ecosystem sentinels: developing a health monitoring system. *EcoHealth*, *1*, 246–254. https://doi.org/10.1007/s10393-004-0094-6

Wiley, D. N., Zadra, C. J., Friedlaender, A. S., Parks, S. E., Pensarosa, A., Rogan, A., Shorter, K. A., Urbán, J., & Kerr, I. (2023). Deployment of biologging tags on free swimming large whales using uncrewed aerial systems. *Royal Society Open Science*, *10*(4), Article 221376. https://doi.org/10.1098/rsos.221376

SUPPORTING INFORMATION

Additional supporting information can be found online in the Supporting Information section at the end of this article.

How to cite this article: Yang, D. Y., Shorter, K. A., Moore, M., Rocho-Levine, J., Wells, R. S., Barton, K., & Johnson, M. (2025). In vivo viscoelastic properties of cetacean integument: an experimental characterization. *Marine Mammal Science*, *41*(1), e13153. https://doi.org/10.1111/mms.13153